Appl Nanosci (2016) 6:691–702
DOI 10.1007/s13204-015-0474-y

ORIGINAL ARTICLE

$TiInCrO_6$-nanomaterial synthesis, characterization and multi applications

J. Kamalakkannan[1] · V. L. Chandraboss[1] · B. Loganathan[1] · S. Prabha[1] · B. Karthikeyan[1] · S. Senthilvelan[1]

Received: 16 April 2015 / Accepted: 16 June 2015 / Published online: 15 July 2015

Abstract In this article, we reported the highly reusable undoped titanium dioxide and doped $TiInCrO_6$ nanomaterial by simple precipitation method and sonication technique. The prepared nanomaterials were characterized by X-ray diffraction, field-emission scanning electron microscopy with elementary dispersive X-ray, high-resolution transmission electron microscopy, techniques and ultraviolet and visible-diffuse reflectance studies. The influence of operational parameters such as the effect of catalyst loading dye concentration and chemical oxygen demand measurements had also been investigated. The synthesized $TiInCrO_6$ nanomaterial was proposed as the promising photocatalyst for the degradation of rhodamine B (Rh B) dye and reusability. The mechanism of the photocatalytic effect of the $TiInCrO_6$ nanomaterial has been discussed. Thus, the use of $TiInCrO_6$ in water purification showed potential. The photodegradation of Rh B dye was well described by pseudo-first-order kinetics and high quantum yield. The photovoltaic characterization had been studied, cyclic voltammogram measurements. The antibacterial activity of the prepared nanomaterials had been investigated against Gram negative *Escherichia coli* and Gram positive *Staphylococcus aureus* bacterial strains.

Keywords Nanomaterial · Electronic microscopic analysis · Photocatalysis · Photovoltaic characterization · Cyclic voltammogram (CV) · Antibacterial activity

✉ S. Senthilvelan
dr_senthilvel@yahoo.co.in

[1] Department of Chemistry, Annamalai University, Annamalainagar 608 002, India

Introduction

Rhodamine B (Rh B) dye is useful in many industries such as paper, cosmetics, food and textiles. This dye is used to colorize the foodstuffs. The dye and its degradation products such as aromatic amines are greatly carcinogenic and hazardous. Advanced oxidation process is a photocatalysis in waste water treatment technique and it is used for the total mineralization of organics (Alaei et al. 2012; Mills and Lee 2002). Titanium dioxide (TiO_2) is a smart oxide semiconducting material and is greatly studied in the field of environmental water technologies. Remaining nontoxicity, superior redox ability, availability and photodegradation stability of it are also studied (Jiang et al. 2014; Liu et al. 2009; Yang et al. 2008, 2009; Han et al. 2009; Wu et al. 2008). The photocatalytic activity of a multimetal oxide system also depends on their compositions in the current year. The twofold metal oxides such as for TiO_2/Fe_2O_3, TiO_2/SiO_2 TiO_2/MoO_3, TiO_2/WO_3 and TiO_2/ZrO_2 have been generally considered for their single chemical, physical and photocatalytic properties (Ghorai et al. 2011; Do et al. 1994; Papp et al. 1994; Xu et al. 2012; Fu et al. 1996).

Jiang Yin et al. article reported that $MCrO_4$ (M = Ba and Sr) had shown promising photocatalytic properties (Yin et al. 2003; Tanmay et al. 2013). Surface sensitization by organic dye molecules was reported recently (Zhang et al. 2013; Park et al. 2010; Le et al. 2012). In the present work, the preparation of TiO_2 and $TiInCrO_6$ and their characterization by suitable analytical methods is discussed. It aims to enhance the photocatalytic, of TiO_2 and study of $TiInCrO_6$ using spray pyrolysis method for photovoltaic application, cyclic voltammeter and bacterial strains (Scheme 1).

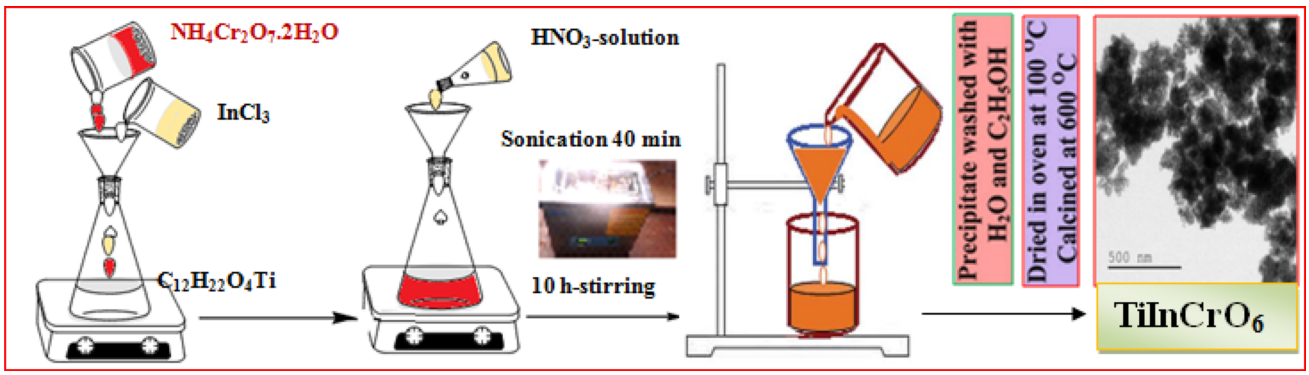

Scheme 1 Preparation of $TiInCrO_6$ nanomaterial

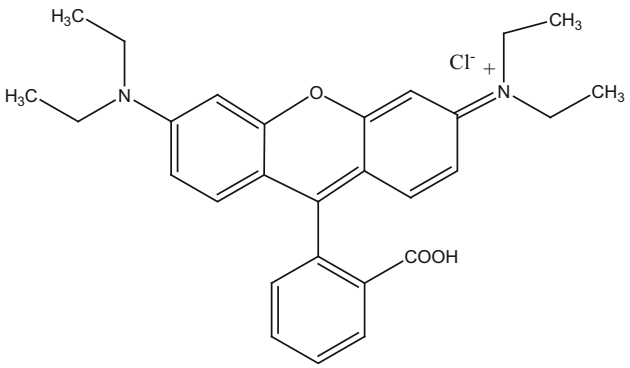

Fig. 1 Chemical structure of rhodamine B

Experimental

Materials

Tetra isopropyl orthotitanate, ammonium dichromate dihydrate, indium chloride, NH_3 solution, nitric acid-65 %, rhodamine B ($C_{28}H_{31}ClN_2O_3$) are used and is shown in Fig. 1. A gift sample of TiO_2-P25 (80 % anatase) and ethanol, the guaranteed reagents of Sigma Aldrich and deionized water is used as a solvent throughout the experiment.

Synthesis of $TiInCrO_6$ nanomaterial

$TiInCrO_6$ nanomaterial was synthesized by the precipitation method. The 1:1 amount of $InCl_3$ and $((NH_4)_2Cr_2O_7 \cdot 2H_2O$ were first dissolved with deionized water. The resulting solution ($InCrO_4$) was added dropwise into tetra isopropyl orthotitanate solution at room temperature. The above solution was vigorous by stirred for 4 h and than 2–3 drops of conc. nitric acid and 5 mL deionized water were added. The obtained solution was stirred for 2 h and ultrasonication was done for 20 min, until precipitate was formed. The precipitate was washed with deionized water and ethanol. Then the precipitate was collected and dried in oven at 100 °C for 12 h. The obtained material was finally calcined at 600 °C for 2 h, to achieve $InCrO_4$ doped-TiO_2 and finally it was calculated as $TiInCrO_6$ nanomaterial.

Characterization

X-ray diffraction (XRD) spectra were recorded on the X'PERT PRO model X-ray diffractometer from Pan Analytical instruments operated at a voltage of 40 kV and a current of 30 mA with Cu Kα radiation The morphological observation of the prepared materials were made by field-emission scanning electron microscopy (FE-SEM) with elementary dispersive X-ray (EDX) analysis and it was carried out on a FEI Quanta FEG 200 instrument with EDX analyzer facility at 25 °C. The sample was prepared by placing a small quantity of prepared material on a carbon-coated copper grid and allowing the solvent to evaporate by high resolution transmission electron microscopy (HR-TEM), TECNAI G2 FEI F12 model. The crystallinity was characterized by an ultraviolet and visible (UV–vis) DRS and the direct band gap energy was analyzed by UV–visible (Shimadzu UV-1650 PC) spectrophotometer. UV–vis absorbance spectra were measured over a range of 800–200 nm with a Shimadzu UV-1650PC recording spectrometer using a quartz cell with 10 mm of optical path length. The antibacterial activity was studied by disc diffusion method. The test compound was dissolved in DMSO (200 mg/mL) for about half an hour. Commercially available drug disc, ciprofloxacin (10 mg/disc), was used as positive reference standard, and photovoltaic properties of

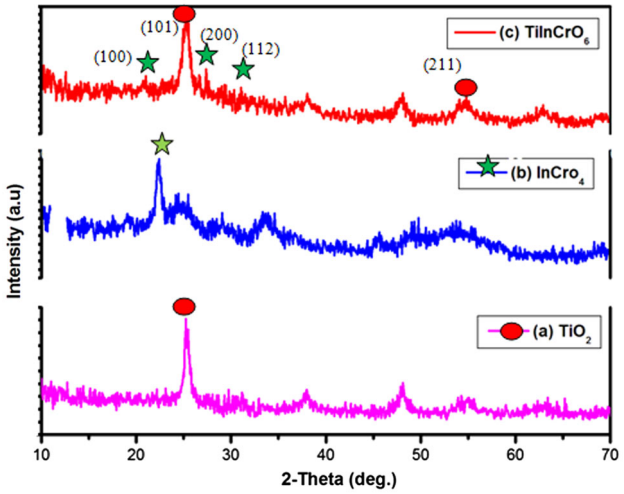

Fig. 2 XRD analysis **a** TiO_2, **b** $InCrO_4$ and **c** $TiInCrO_6$ nanomaterial

the material were characterized by recording the photo current–voltage curve under illumination of A.M.1.5 (100Mw/cm^2) and cyclic voltammetry (CV) measurements were carried out using CHI 60 AC electrochemical analyzer (CHI Instruments Inc., USA).

Results and discussion

XRD analysis

XRD spectra were recorded and peaks at 25.22 and 54.27 are the diffractions from the TiO_2 (101) and (211) crystal planes. Diffractions peaks of anatase phase TiO_2 (JCPDS No. 21-1272) is shown in Fig. 2a. In Fig. 2b highest diffractions peaks at 22°, 27° and 29° are diffraction of the $InCrO_4$ (100), (200) and (112) crystal planes diffractions peaks of $InCrO_4$ (JCPDS No. 01-088-0110). The samples of $InCrO_4$ doped-TiO_2 are present in $TiInCrO_6$ (Fig. 2c) exhibits a diffraction pattern of FCC crystal structure. The average crystalline size (L) of the TiO_2, $InCrO_4$ and $TiInCrO_6$ particles have been calculated from the Debye–Scherrer formula, $L = 0.89\lambda/\beta \cos\theta$ where L is the crystalline size (in nm), l is the wavelength (in nm), b is the full width at half maximum intensity (FWHM-in radian), and u is the Bragg diffraction angle (θ). The average crystalline size of prepared TiO_2 and $InCrO_4$ material was compared and figured out to be about 80 and 75 nm. The average crystalline sizes of $TiInCrO_6$ nanomaterial are almost 30 nm. This is consistent with the crystallite size estimated from the XRD analysis.

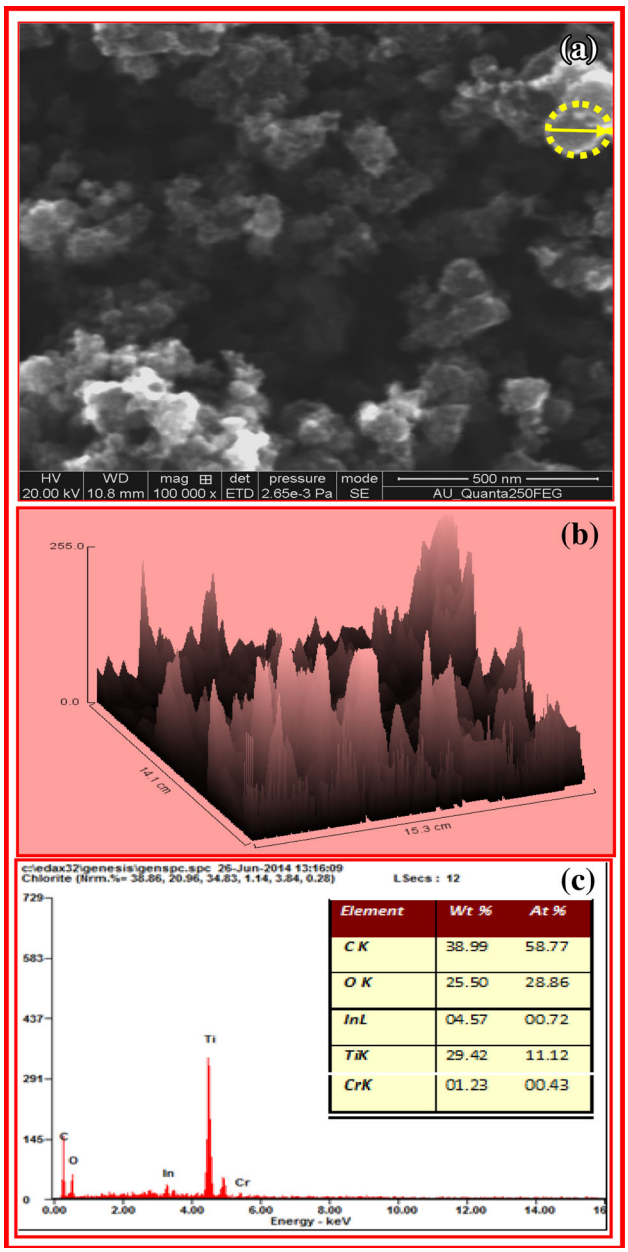

Fig. 3 Field-emission scanning electron microscopy (FE-SEM). **a** SEM image, **b** surface plot selected area highlighted in fig. **a**, **c** Energy-dispersive X-ray (EDX) elemental data of $TiInCrO_6$ nanomaterial

Electronic microscopic analysis

FE-SEM analysis

Figure 3a shows the FE-SEM image of $TiInCrO_6$ nanomaterial. It is shown that there is a modification in the

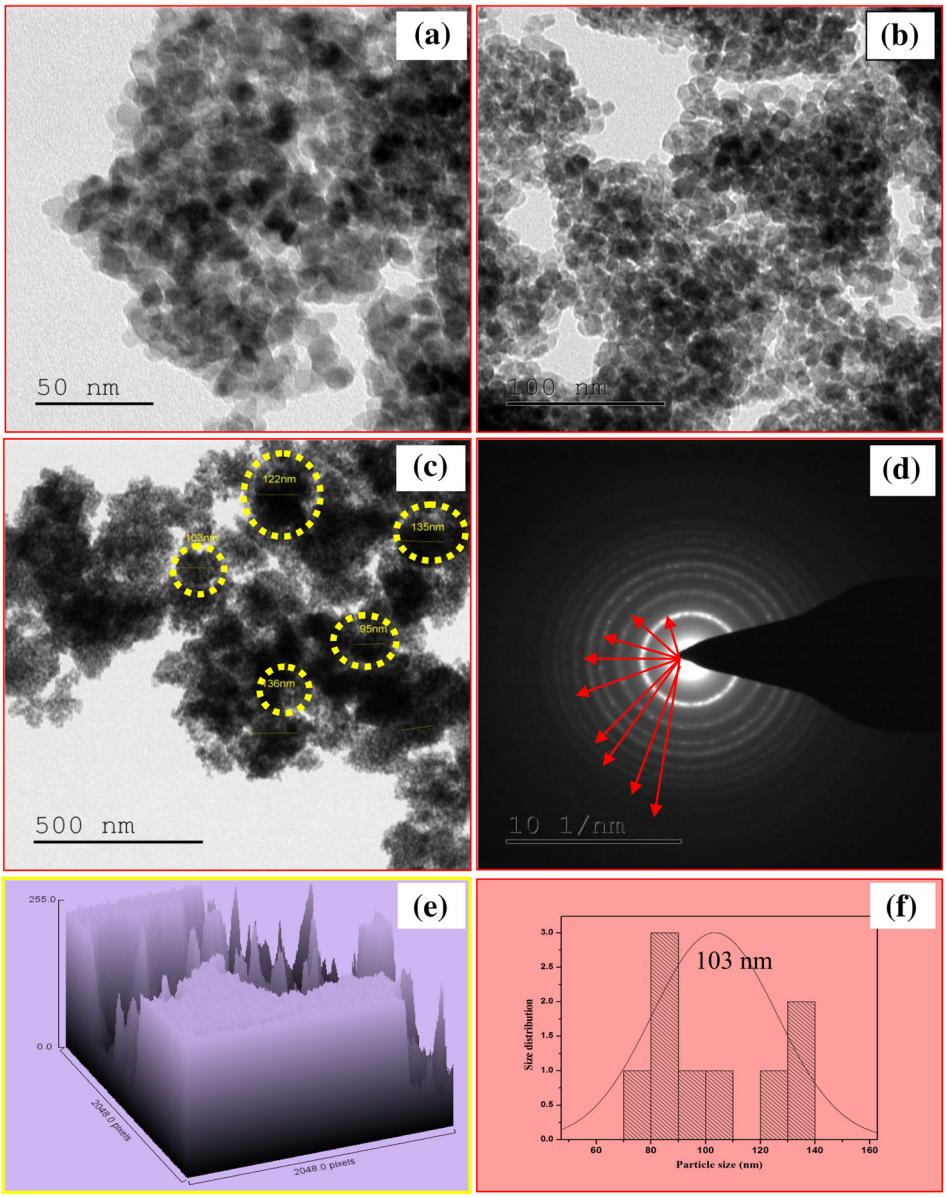

Fig. 4 **a–c** High-resolution transmission electron microscopy (HR-TEM) images of $TiInCrO_6$ nanomaterial, **d** SAED pattern, **e** surface plot and **f** particle size selected area highlighted in **c**, particle size distribution of $TiInCrO_6$ nanomaterial

surface morphology spherical-shaped structure. The energy dispersive X-ray analysis shows that the presence of In, Cr, Ti and O in $TiInCrO_6$ nanomaterial is shown in Fig. 3b. Figure 3a shows the length of the selected particles area using the ''Image J Viewer" software (Loganathan et al. 2015) by surface plot is shown in Fig. 3c.

HR-TEM analysis

The synthesized $TiInCrO_6$ nanomaterial has a well clear spherical-shaped structure in the HR-TEM micrograph. These micrographs in Fig. 4a–c clearly showed the spherical-shaped particles. The selected area electron diffraction (SAED) pattern of the spherical-shaped $TiInCrO_6$ nanomaterial (Fig. 4d) showed nine diffraction bright rings corresponding to the nine different crystal planes of spherical-shaped structure (with a space of 2.1, 3.5, 5, 5.5, 6.4, 7.5, 8, 8.5 and 9.1 1 nm/1, correspondingly polycrystalline nature). Figure 4e, f represents image profile and particle size distribution (in nm), respectively, of the obtained nanomaterial. The average particle size 103 nm and the selected particles are highlighted in Fig. 4c.

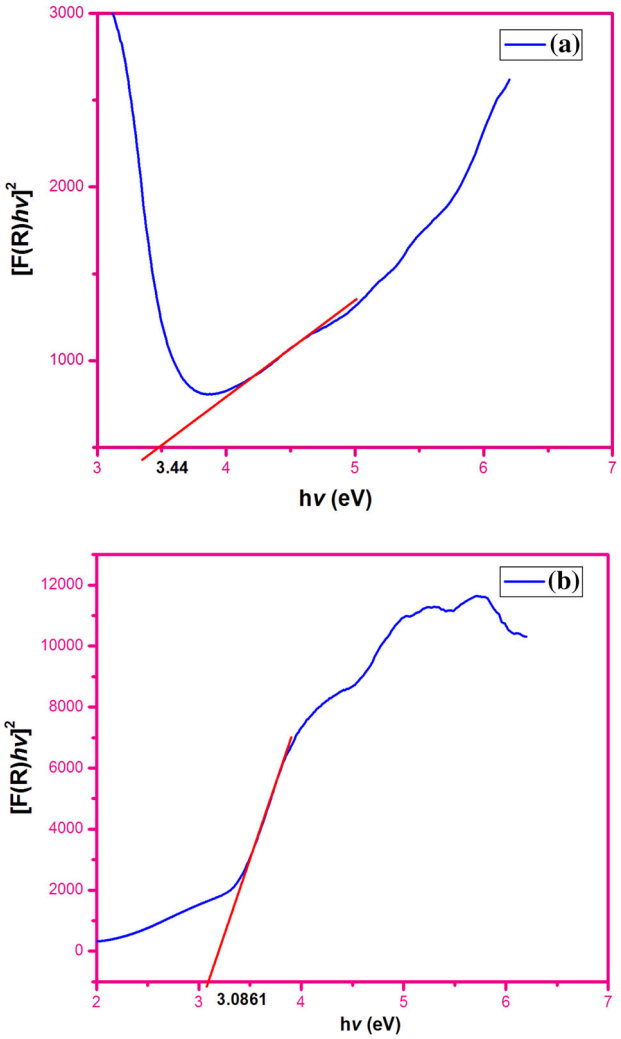

Fig. 5 UV–vis DRS—direct band gap energy **a** TiO_2 and **b** $TiInCrO_6$ nanomaterial

UV–vis-DRS analysis

The UV–vis-DRS spectra of undoped TiO_2 and doped $TiInCrO_6$ are shown in Fig. 5a, b. The direct band gaps of the synthesized nanomaterials have been resolute from the Tauc plots. The plots of $[F(R)\ h\nu]^2$ vs the photon energy ($h\nu$) give the direct band gap of the synthesized TiO_2 and $TiInCrO_6$ as 3.44 and 3.06 eV, correspondingly. The UV–vis-DRS consequences confirm a decrease in the direct band gap of $TiInCrO_6$ compare to that of TiO_2. These results expose $TiInCrO_6$ determination to be functional as an effective photocatalyst.

Preliminary analysis and kinetic study

The initial dye concentration (1×10^{-4} M) in 50 mL solution of Rh B and the catalyst loading is 0.150 g by UV light irradiation at 365 nm. The $TiInCrO_6$ material shows superior photocatalytic activity when compare to that of undoped TiO_2 and TiO_2-P25 in, Dark and nil catalyst. Reaction of Rh B undergoes % of degradation from 0, 22.4, 43.9, 61, 80.5 and 89 % in the presence of $TiInCrO_6$ under UV light at 365 nm in 75 min irradiation is shown in Fig. 6a, b. The stability and reusability of the $TiInCrO_6$ nanomaterial are achieved investigated by repeating Rh B degradation experiments six more times. After each cycle the $TiInCrO_6$ photocatalysts were washed thoroughly with water, and a fresh solution of Rh B was made before every run in the photoreactor. The complete degradation occurs in the 1st, 2nd, 3rd, 4th, 5th and 6th cycle. The complete degradation occurs in the 1st cycle (100%), 2nd cycle (98%), 3rd cycle (97%), 4th cycle (96%), 5th cycle (95%) and 6th cycle (95%). The result indicates that the prepared catalysts are stable and reusable. After the completion of the degradation process, the solution is tested for In^{3+} by leaching with Na_2S. There is no precipitation of In^{3+} S (black color) was formed. As there is no further leaching of In^{3+}, this material is non-hazardous for wastewater treatment (Balachandran and Swaminathan 2012). In Fig. 6c, the rate is calculated by measuring the time reliant degradation efficiency of Rh B in an aqueous material suspension under UV light irradiation contact. For this reason Rh B itself is a dye which is more active to UV light absorbtion. Its photocatalytic degradation is in the order of the catalyst material $TiInCrO_6 > TiO_2$. The photodegradation kinetics study of Rh B on TiO_2 and $TiInCrO_6$ are calculated using the pseudo-first-order kinetics model Eq. (1)

$$\ln(C_0/C_t) = \mathrm{Kapp}^t, \tag{1}$$

where Kapp^t is the rate constant (min), C_0 is the initial concentration of Rh B, and C_t is the concentration of Rh B at reaction time (t) (Zhang et al. 2014; Chandraboss et al. 2015) from the results (Fig. 6d), $TiInCrO_6$ shows the maximum degradation rate constant, around ($1.6361 \times 10^{-4}\ s^{-1}$) which is higher than that of TiO_2 ($1.023 \times 10^{-4}\ s^{-1}$). The photodegradation rate constants (k') of Rh B dye in the monochromatic light source yields reaction quantum yield (Subash et al. 2013a, b; Daneshvar et al. 2007; Choy and Chu 2007) by following Eq. (2).

$$\Phi = \frac{k}{2.303 I_{0,\lambda} \varepsilon_{D\lambda} l} \tag{2}$$

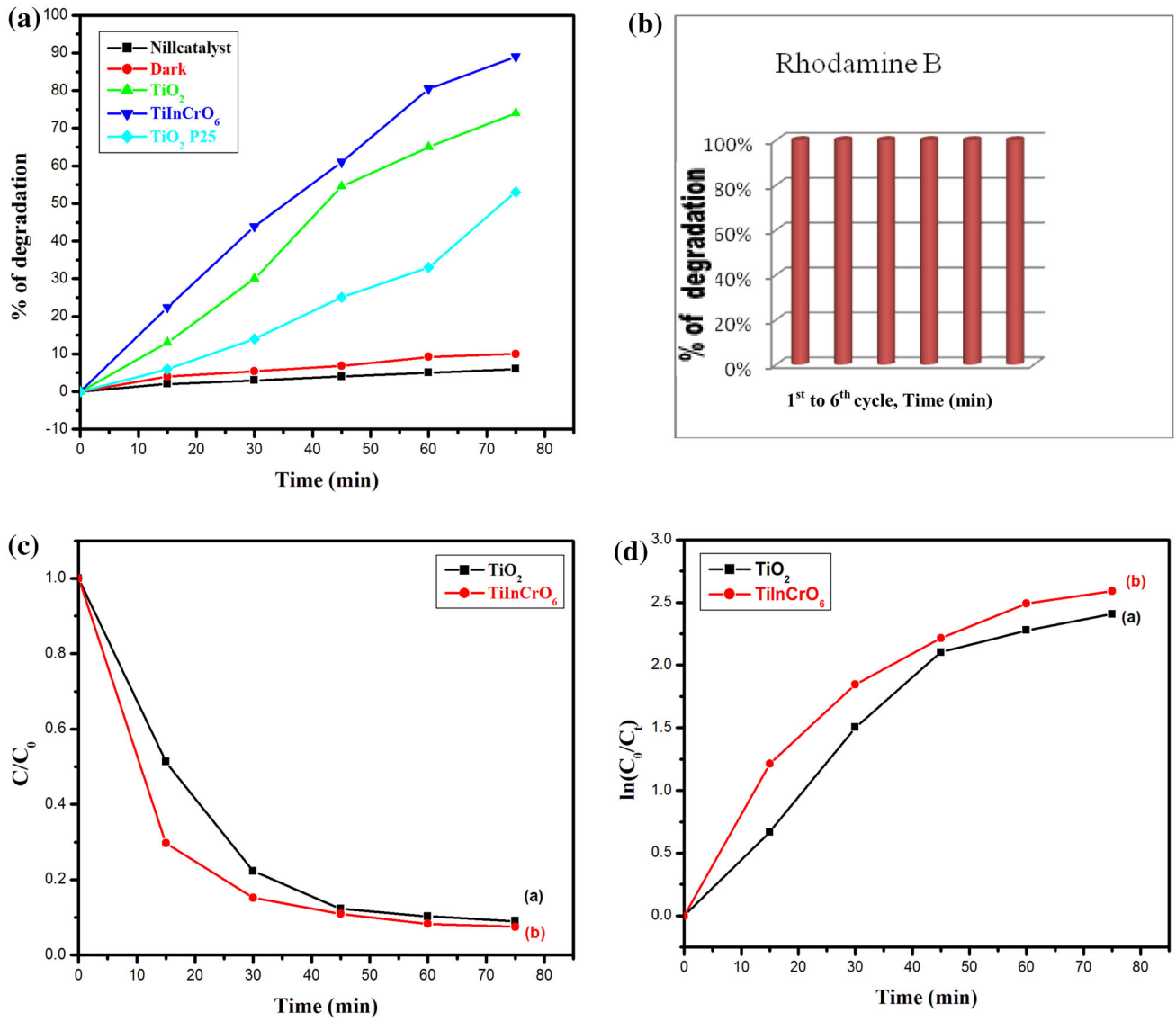

Fig. 6 **a** Primary analysis, **b** reusability of $TiInCrO_6$ on Rh B dye, **c** kinetic of Rh B dye degradation upon irradiation and **b** photodegradation efficiency in undoped TiO_2 and doped $TiInCrO_6$, variations in $\ln(C_0/C)$ as purpose of irradiation time and linear plot of catalysts

where Φ is the reaction of quantum yield (dimensionless), I_o is the light intensity of the incident light range at 200–800 nm range (1.381×10^{-6}), $\varepsilon_{D\lambda}$ is the molar absorptivity of Rh B at 560 nm (3.192×10^4 cm^{-1} M^{-1}) and (l) is the path length of the reaction tube and is 0.24 m for 50 mL of irradiated solution. The final results of degradation quantum yields by, $TiInCrO_6$ and TiO_2 are 0.0663 and 0.0414, respectively. These results indicate that the quantum yield of the $TiInCrO_6$ process is elevated when compare to TiO_2 nanomaterial.

Mechanism

Scheme 2 shows the general mechanism of the photodegradation of Rh B dye by modified semiconducting oxide $TiInCrO_6$ under active UV light source. The energy of incident photons is greater than the band gap energy. The excitation of valence band electrons then promotes the potential reactions. The incident of the photocatalytic surface area with enough energy leads to the arrangement of a positive hole (hv^+) into the valence

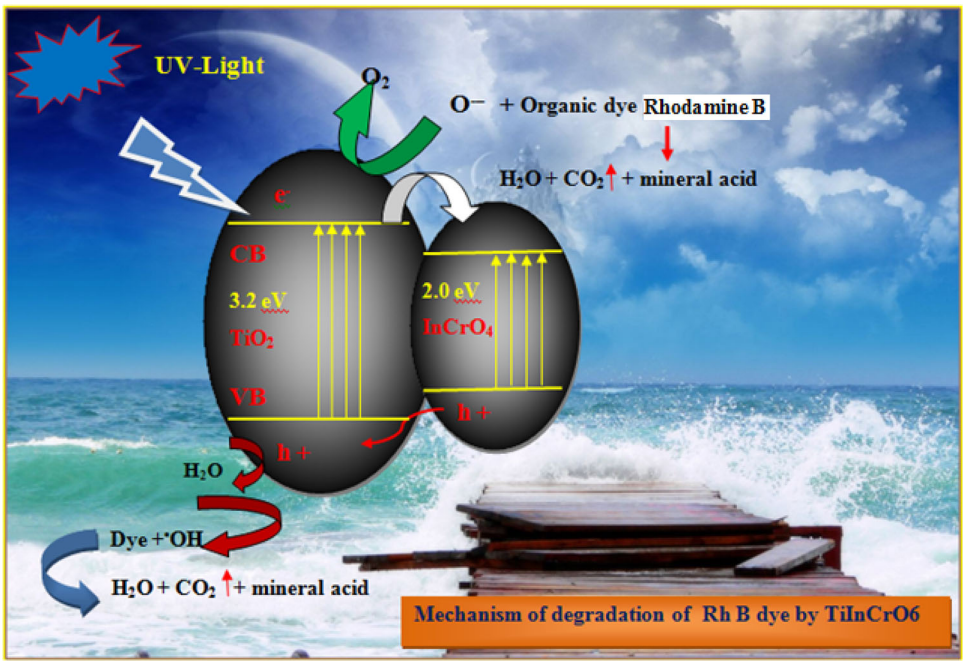

Scheme 2 Schematic diagram of photodegradation of Rh B on $TiInCrO_6$ nano material under UV light for successive mineralization

band and an electron (e^-) through the conduction band. The hole in the valence band reacts with the surface H_2O molecule to generate hydroxyl radicals which reacts with the Rh B dye molecule to degrade the dye.

Effect of catalyst loadings and different concentrations

The different catalyst loading of $TiInCrO_6$ on Rh B has been expected out in the range of 0.100 and 0.150. The total volume of reaction solution is 50 mL, the various amounts of the catalyst loaded in the reaction medium leads to increase the degradation rate. The rate is linearly related to the amount of catalyst loading. Among the three loadings 0.150 g has shown better activity and rapid degradation when compare to other catalyst loading. The effect of different dye concentrations (1×10^{-4} and 1×10^{-5}) is also investigated under UV light is shown in Fig. 7a. It reveals that the increase in dye concentration leads the activity is decrease. Photodegradation of Rh B more in lesser concentration, when compare to high concentration (Fig. 7b).

Chemical oxygen demand (COD) analysis

Mineralization of $TiInCrO_6$ (0.150 g) on Rh B dye (1×10^{-4}) suspension 50 mL pH 7 Solution and air passing with UV light irradiation by COD analysis. The percentage of COD reduction is specified in Fig. 8. After 0, 15, 30, 45, 60 and 75 min irradiation, 0, 25, 46, 59, 82 and 93 % of COD measurements reduction is obtained. This indicates the total mineralization of dye. The mineralization is also specific by formation of calcium carbonate when the evolved gas (CO_2) through degradation is accepted and calcium hydroxide solution is obtained (Subash et al. 2013a, b).

Photovoltaic characterization

Figure 9 shows the photo current–voltage (J–V) characteristics of the dye sensitized solar cell (DSSCs). The undoped TiO_2 and $InCrO_4$ doped-TiO_2 act as photoelectrode are coated on fluorine doped tin oxide (FTO-plate) glass substract. The routine parameter of solar cell is fabricated with TiO_2 and $TiInCrO_6$ with ruthenium dye (535-bisTBA, N719). From the data, it is clear that (N719) with $TiInCrO_6$-based cell gives the most brilliant performance with the use of dye as sensitizer reunite the highest value of short-circuit current density, Jsc (4.1 mA/cm^2), open-circuit voltage, Voc (500 mV), fill-factor, FF (0.94 and efficiency, η (1.7 %). It is observed that the effectiveness of doped photoelectrode-based cell is much higher than TiO_2 (Liu et al. 2010; Zhang et al. 2011).

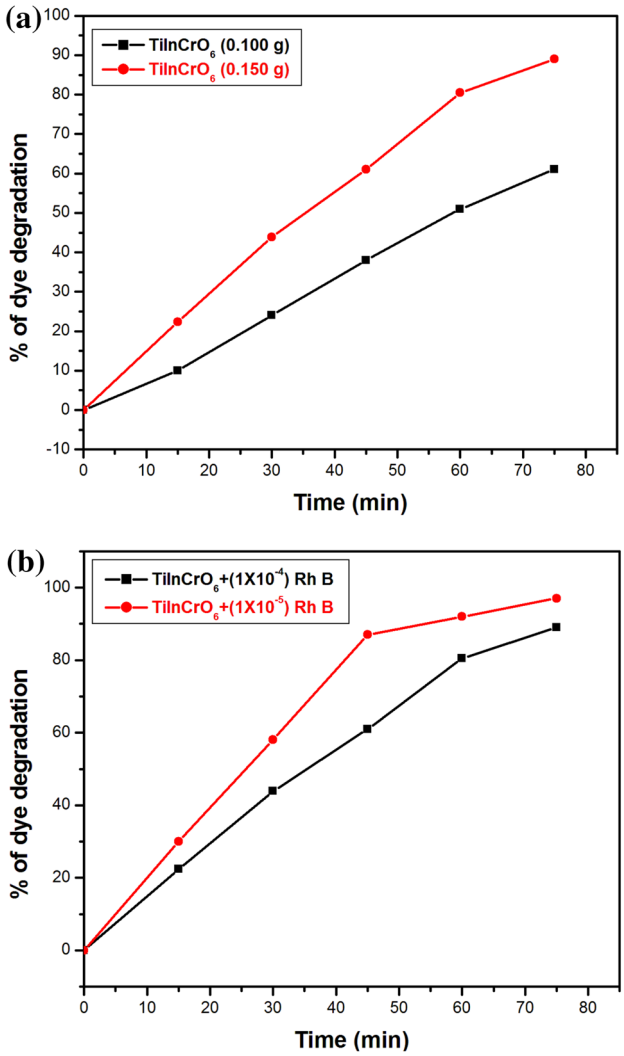

Fig. 7 **a** Effect of catalyst loading and **b** effect of dye different concentrations

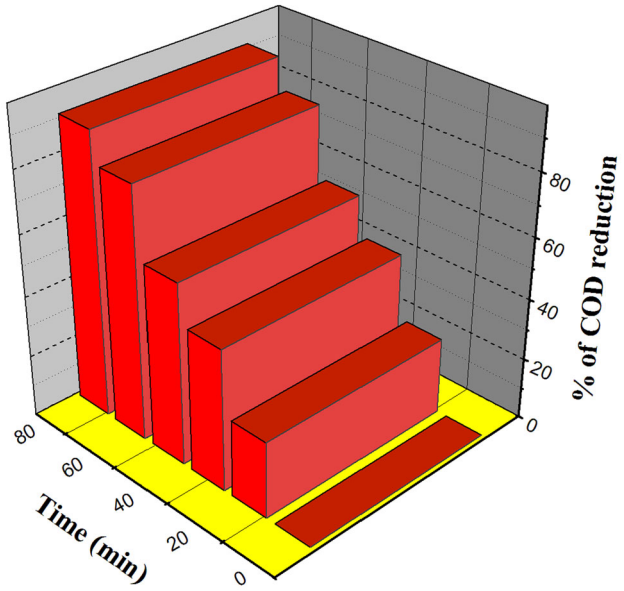

Fig. 8 Chemical oxygen demand (COD) analysis of $TiInCrO_6$ nanomaterial

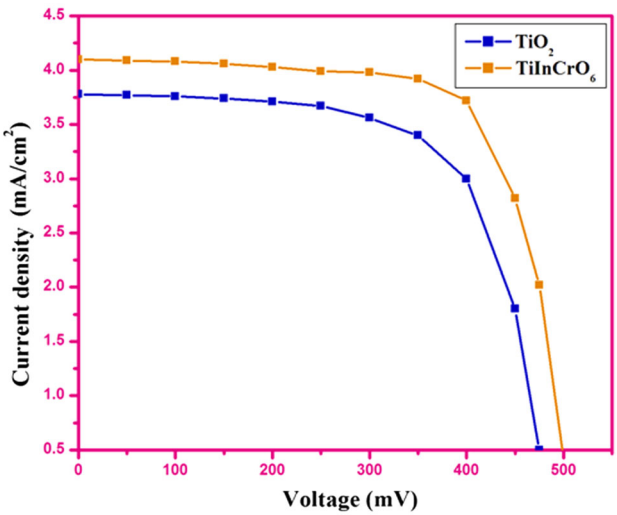

Fig. 9 Current density–voltage (J–V) curves for the dye sensitized solar cell (DSSCs) fabricated from TiO_2 and $TiInCrO_6$ nanomaterial

Antibacterial activity

The bacterial strains viz., (a) *Escherichia coli* (*E. coli*) that is a Gram-negative and (b) *Staphylococcus aurous* (*S. aurous*) that is a Gram-positive, are used in this investigation (Ariharan and Nagendra Prasad 2014). DMSO is used as control while ciprofloxacin is used as. The $TiInCrO_6$ nanomaterial is tested against the bacterial strains from the zone of inhibition of the antibacterial activity. The $TiInCrO_6$ (2) nanomaterial against (a) *E. coli*, (b) *S. aurous* shows better activity than TiO_2 (1), is shown in Fig. 10 and Table 1. That $TiInCrO_6$ nanomaterial has better performance viz photovoltaic properties, photocatalytic activity and antibacterial activity.

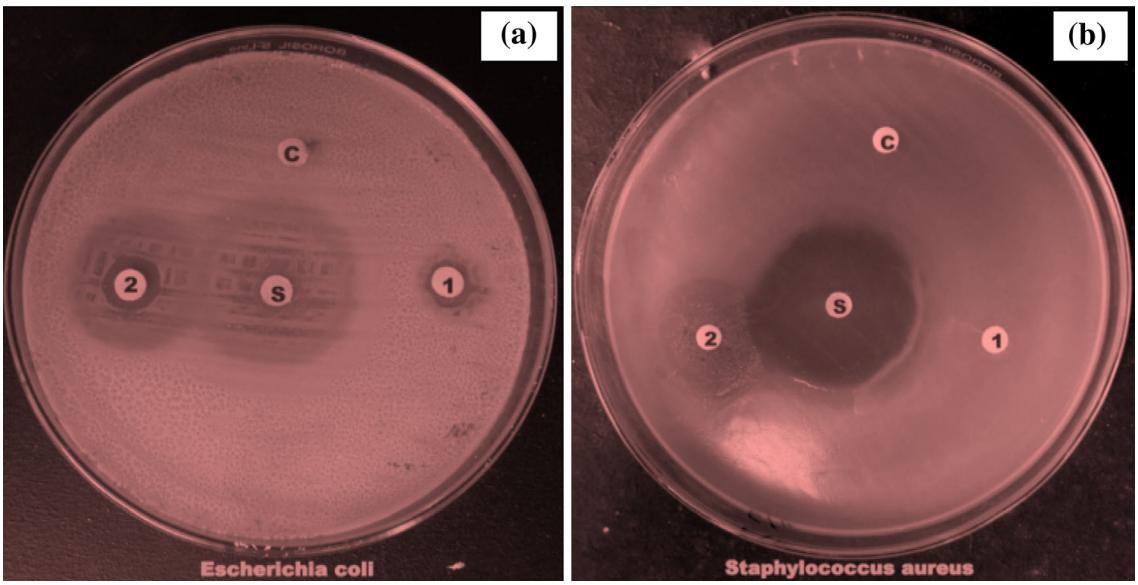

Fig. 10 Antibacterial activity (disc diffusion method) **a** *Escherichia coli,* **b** *Staphylococcus aurous* investigation of TiO_2 and $TiInCrO_6$ nanomaterial

Table 1 Antibacterial activity (disc diffusion method)

	Bacteria	Standard antibiotic disk[a]	Zone of inhibition (nm)		
			$[TiO_2]$	$[TiInCrO_6]$	Control (DMSO)
1	*Staphylococcus aureus*	26	09	23	–
2	*Escherichia coli*	28	10	24	09

[a] Ciprofloxacin

Cyclic voltammogram (CV)

The prepared photocatalyst is a surface occurrence as the photogenerated charge carriers scatter to the surface to begin redox reactions (Sajjad et al. 2013). Prepared nanomaterial TiO_2 and $TiInCrO_6$ using modified electrode is constructed through the mechanical attachment. Figure 11 shows the cyclic voltammogram of unmodified/modified glassy carbon electrode on the electrochemical oxidation/reduction potential. After the glassy carbon electrode was not made to order within the least prepared photocatalyst, at give is hardly every enrichment or decrement in the cycles. The mashered amid TiO_2 modified glassy carbon electrode, it be investigational that the electrochemical oxidation of KCl is an irreversible process suitable to the peak [anodic current and the (Epa) peak potential of 0.0233 V and $i = 1.627\ e^{-5A}$]. Although $TiInCrO_6$ modifies glassy carbon electrode, the deficiency of a well-defined reduction glassy carbon electrode was showing that the electrochemical redox reaction of KCl is a reversible process [enhanced anodic current and the (Epa) peak potential of 0.350 V, and $i = 3.334\ e^{-5A}$]. These results are (segment = 1 to segment = 40) shown in Fig. 12 indicates that $TiInCrO_6$ modified glassy carbon electrode has larger adsorption–desorption and high electrochemical reaction than that of TiO_2 nanomaterial. A few literature information has indicated that glassy carbon electrodes modified with metal ion and carbon materials are created to achieve enhanced in comparison to bare GCE (Subash et al. 2013a, b; Zidan et al. 2010; Radhi et al. 2010; Chandraboss et al. 2015). The result thus suggests that the occurrence of could increases current and improves the relation electron transferred by $TiInCrO_6$ nanomaterial.

Conclusion

In summary, we had successfully synthesized $TiInCrO_6$ nanomaterial by simple precipitation method. It was characterized by XRD, FE-SEM with EDX, HR-TEM

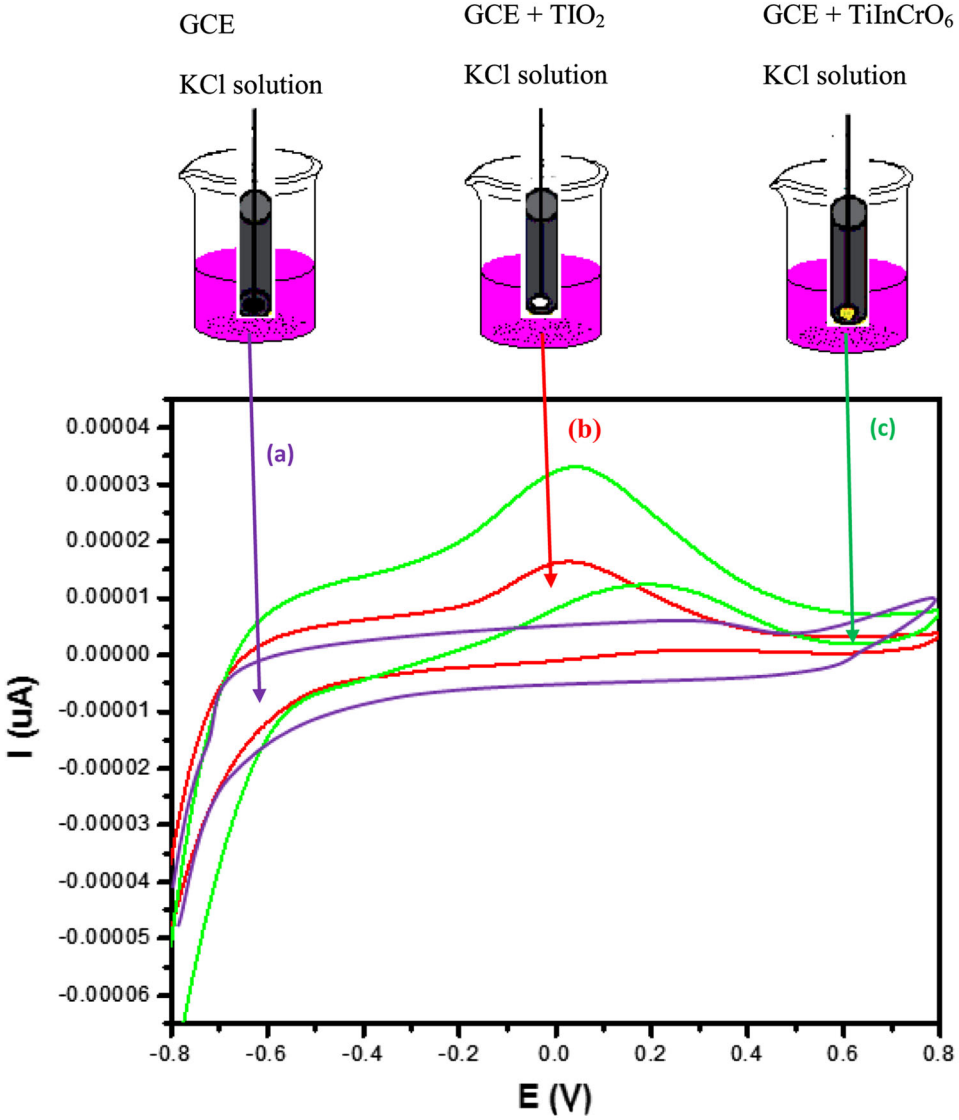

Fig. 11 CVs of **a** uncoated GCE with 0.1 M KCl (*violet curve*), **b** TiO_2 coated GCE in 0.1 M KCl (*red curve*) and **c** $TiInCrO_6$ coated GCE in 0.1 M KCl (*green curve*)

analysis. FE-SEM and HR-TEM image showed the $TiInCrO_6$ had spherical-shaped structure. EDX spectra definite this revealed the presence of Ti, In, Cr and O in the catalyst. UV–vis-DRS results demonstrated that the decrease in the direct band gap of $TiInCrO_6$ nanomaterial compared to undoped TiO_2 nanomaterial. $TiInCrO_6$ had higher photocatalytic activity and reusability. The influence of operational parameters such as the effect of catalyst loading, dye concentration and COD measurements confirmed complete mineralization of the Rh B molecule. The $TiInCrO_6$ kinetic study was conducted using the pseudo-first-order kinetic model, and the high quantum yield was calculated. The higher Photovoltaic properties of the DSSCs were characterized. The cyclic voltammogram result shows increased current and improves the relation with electron transferred by $TiInCrO_6$ nanomaterial. The mechanism of dye degradation is future for the superior photocatalytic activity and water purification performance is shows $TiInCrO_6$ nanomaterial.

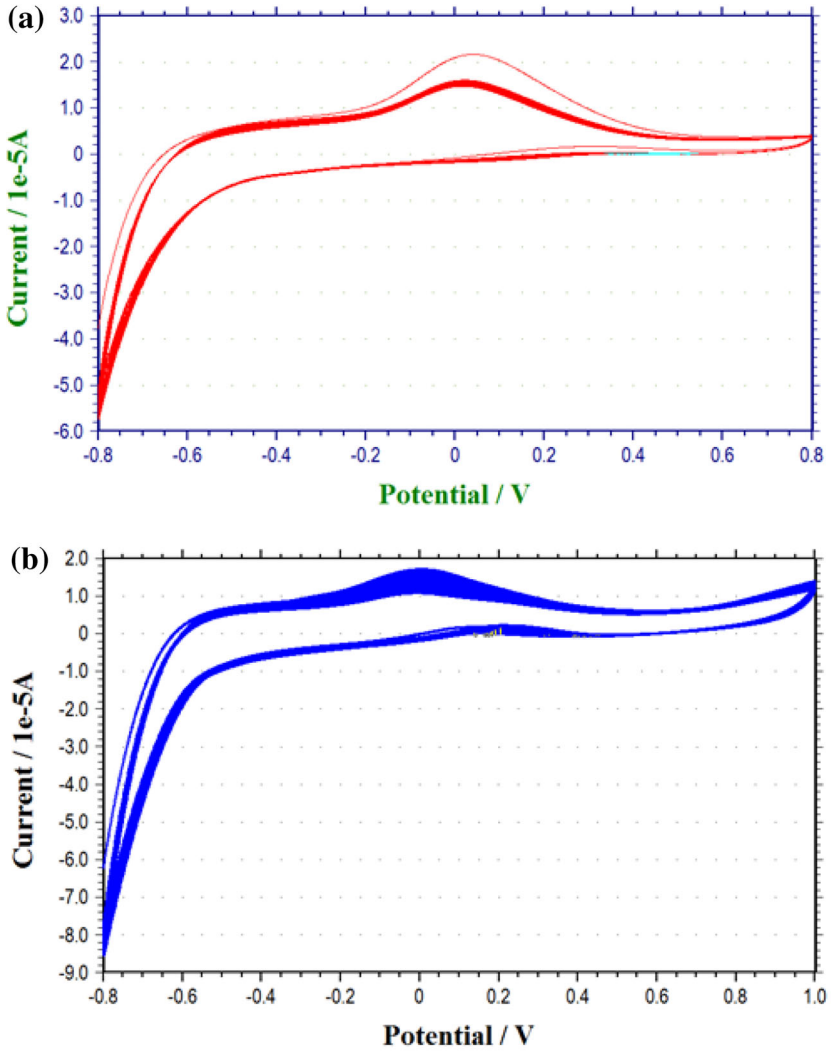

Fig. 12 **a** TiO_2 coated GCE in 0.1 M KCl (*red curves segment* 40) and **b** $TiInCrO_6$ coated GCE in 0.1 M KCl (*blue curves segment* 40)

Compliance with ethical standards

Conflict of interest The authors declare no competing financial interest.

References

Alaei M, Mahjoub AR, Rashidi A (2012) Effect of WO3 nanoparticles on congo red and rhodamine B photo degradation. Iran J Chem Chem Eng 31:23–29

Ariharan VN, Nagendra Prasad P (2014) Anti-bacterial activity of three morphological traits of *Aegle marmelos* (Linn.) Corr.-'vilvam' Rasayan. J Chem 7:260–263

Balachandran S, Swaminathan M (2012) Facile fabrication of heterostructured Bi_2O_3–ZnO photocatalyst and enhanced photocatalytic activity. J Phys Chem C 116:26306–26312

Chandraboss VL, Kamalakkannan J, Prabha S, Senthilvelan S (2015) An efficient removal of methyl violet from aqueous solution by an AC-Bi/ZnO nanocomposite material. RSC Adv 5:25857–25869

Choy WK, Chu W (2007) The use of oxyhalogen in photocatalytic reaction to remove o-chloroaniline in TiO_2 dispersion. Chemosphere, Chemosphere 66:2106–2113

Daneshvar N, Aber S, Dorraji MS, Khataee AR, Rasoulifard MH (2007) Preparation and investigation of photocatalytic properties of ZnO nanocrystals: effect of operational parameters and kinetic study. Int J Chem Nucl Metall Mater Eng 5

Do YR, Lee W, Dwight K, Wold A (1994) The effect of WO_3 on the photocatalytic activity of TiO_2. J Solid State Chem 108:198–201

Fu X, Clark LA, Yang Q, Anderson MA (1996) Enhanced photocatalytic performance of titania-based binary metal oxides: TiO_2/SiO_2 and TiO_2/ZrO_2. Environ Sci Technol 30:647–653

Ghorai Tanmay, Biswas Niladri (2013) Photodegradation of rhodamine 6G in aqueous solution via $SrCrO_4$ and TiO_2 nanosphere mixed oxides. J Mater Res Technol 2:10–17

Ghorai TK, Chakraborty M, Pramanik P (2011) Photocatalytic performance of nano photocatalyst from TiO_2 and Fe_2O_3 by mechanochemical synthesis. J Alloys Compd 509:8158–8164

Han X, Kuang Q, Jin M, Xie Z, Zheng L (2009) Synthesis of titania nanosheets with a high percentage of exposed (001) facets and related photocatalytic properties. J Am Chem Soc 131:3152–3153

Jiang Z, Liu D, Jiang D, Wei W, Qian K, Chen M, Xie J (2014) Bamboo leaf-assisted formation of carbon/nitrogen co-doped anatase TiO_2 modified with silver and graphitic carbon nitride: novel and green synthesis and cooperative photocatalytic activity. Dalton Trans 43:13792–13802

Le TT, Akhtar MS, Park DM, Lee JC, Yang OB (2012) Water splitting on Rhodamine-B dye sensitized Co-doped TiO_2 catalyst under visible light. Appl Catal B 112:397–401

Liu G, Yang HG, Wang X, Cheng L, Pan J, Lu GQ, Cheng HM (2009) Visible light responsive nitrogen doped anatase TiO_2 sheets with dominant {001} facets derived from TiN. J Am Chem Soc 131:12868–12869

Liu J, Yang H, Weiwei T, Zhou X, Lin Y (2010) Photovoltaic performance improvement of dye sensitized solar cells based on tantalum-doped TiO_2 thin films. Electrochim Acta 56:396–400

Loganathan B, Chandraboss VL, Murugavelu M, Senthilvelan S, Karthikeyan B (2015) Synthesis and characterization of multi-metallic-core and siliceous-shell Au/Pt/Ag@SiO_2 sol–gel derived nanocomposites. J Sol–Gel Sci Technol 74:1–4

Mills A, Lee SK (2002) A web-based overview of semiconductor photochemistry-based current commercial applications. J Photochem Photobiol A Chem 152:233

Papp J, Soled S, Dwight K, Wold A (1994) Surface acidity and photocatalytic activity of TiO_2, WO_3/TiO_2, and MoO_3/TiO_2 photocatalysts. Chem Mater 6:496–500

Park Y, Lee SH, Kang SO, Choi W (2010) Organic dye sensitized TiO_2 for the redox conversion of water pollutants visible light. Chem Commun 46:2477–2479

Radhi MM, Tan WT, Rahman MZBA, Kassim AB (2010) Voltammetric detection of Hg (ii) at C_{60} activated carbon and CWCNT modified glassy carbon electrode. Res J Appl Sci 5:59–64

Sajjad S, Leghari SAK, Zhang J (2013) Nonstoichiometric Bi_2O_3: efficient visible light photocatalyst. J RSC Adv 3:1363–1367

Subash B, Krishnakumar B, Sreedhar B, Swaminathan M, Shanthi M (2013a) Highly active WO_3–Ag–ZnO photocatalyst driven by day light illumination. Superlattices Microstruct 54:155–171

Subash B, Krishnakumar B, Swaminathan M, Shanthi M (2013b) Highly efficient, solar active, and reusable photocatalyst: Zr-loaded Ag–ZnO for reactive red 120 dye degradation with synergistic effect and dye-sensitized mechanism. Langmuir 29:939–949

Wu B, Guo C, Zheng N, Xie Z, Stucky GD (2008) Highly efficient photocatalyst: TiO_2 microspheres produced from TiO_2 nanosheets with a high percentage of reactive {001} facets. J Am Chem Soc 130:17563–17567

Xu L, Steinmiller EMP, Skrabalak SE (2012) Achieving synergy with a potential photocatalytic Z-scheme: synthesis and evaluation of nitrogen-doped TiO_2/SnO_2 composites. J Phys Chem C 116:871–877

Yang HG, Sun CH, Qiao SZ, Zou J, Liu G, Smith SC, Cheng HM, Lu GQ (2008) Anatase TiO_2 single crystals with a large percentage of reactive facets. Nature 453:638–641

Yang HG, Liu G, Qiao SZ, Sun CH, Jin YG, Smith SC, Zou J, Cheng HM, Lu GQ (2009) Solvothermal synthesis and photoreactivity of anatase TiO_2 nanosheets with dominant {001} facts. J Am Chem Soc 131:4078–4083

Yin J, Zou Z, Ye J (2003) Photophysical and photocatalytic properties of new photocatalysts MCrO4 (M = Sr, Ba). Chem Phys Lett 378:24–28

Zhang Y, Wang L, Liu B, Zhai J, Fan H, Wang D, Lin Y, Xie T (2011) Synthesis of Zn doped TiO_2 microspheres with enhanced photovoltaic performance and application for dye sensitized solar cells. Electrochim Acta 56:6517–6523

Zhang G, Teng F, Wang Y, Zhang P, Gong C, Chen L, Zhao C, Xie E (2013) Preparation of carbon–TiO_2 nanocomposites by a hydrothermal method and their enhanced photocatalytic activity. RSC Adv 3:24644–24649

Zhang S, Li J, Zeng M, Li J, Xu J, Wang X (2014) Bandgap engineering and mechanism study of nonmetal and metal ion codoped carbon nitride: C + Fe as an example. Chem-A Eur J 20:9805–9812

Zidan M, Tan WT, Zainal Z, Abdullah AH, Goh JK (2010) Electrocatalytic oxidation of ascorbic acid mediated by lithium doped microparticles Bi_2O_3/MWCNT modified glassy carbon electrode. Int J Electrochem Sci 5:501–508